Biointerphases (2012) 7:61
DOI 10.1007/s13758-012-0061-7

ARTICLE

Surface Functionalized Nanofibrillar Cellulose (NFC) Film as a Platform for Immunoassays and Diagnostics

Hannes Orelma · Ilari Filpponen · Leena-Sisko Johansson · Monika Österberg · Orlando J. Rojas · Janne Laine

Received: 21 August 2012 / Accepted: 20 September 2012 / Published online: 3 October 2012
© The Author(s) 2012. This article is published with open access at Springerlink.com

Abstract We introduce a new method to modify films of nanofibrillated cellulose (NFC) to produce non-porous, water-resistant substrates for diagnostics. First, water resistant NFC films were prepared from mechanically disintegrated NFC hydrogel, and then their surfaces were carboxylated via TEMPO-mediated oxidation. Next, the topologically functionalized film was activated via EDS/NHS chemistry, and its reactivity verified with bovine serum albumin and antihuman IgG. The surface carboxylation, EDC/NHS activation and the protein attachment were confirmed using quartz crystal microbalance with dissipation, contact angle measurements, conductometric titrations, X-ray photoelectron spectroscopy and fluorescence microscopy. The surface morphology of the prepared films was investigated using confocal laser scanning microscopy and atomic force microscopy. Finally, we demonstrate that antihuman IgG can be immobilized on the activated NFC surface using commercial piezoelectric inkjet printing.

Electronic supplementary material The online version of this article (doi:10.1007/s13758-012-0061-7) contains supplementary material, which is available to authorized users.

H. Orelma · I. Filpponen (✉) · L.-S. Johansson · M. Österberg · J. Laine
Department of Forest Products Technology, School of Chemical Technology, Aalto University, 00076 Espoo, Finland
e-mail: erkko.filpponen@aalto.fi

O. J. Rojas
Department of Forest Biomaterials, North Carolina State University, Raleigh, NC 27695, USA

1 Introduction

Polymeric materials made from nonrenewable resources have been utilized as support in different medical and diagnostic applications [23, 49, 50]. The commercial utilization of such materials brings about a number of drawbacks, including environmental concerns. Cellulose and its derivatives are viable alternatives to alleviate such issues, due to their inherent properties such as non-toxicity, hydrophilicity, and chemical resistivity [35, 42]; however, their high porosity sets a challenge in diagnostic applications. A cellulose derivative, namely nitrocellulose, has been used as a supporting material for conjugating antibodies in diagnostic assays [26]. However, nitrocellulose has also some limitations including relatively low mechanical strength, flammability, and strong affinity with proteins causing non-specific adsorption [26, 44].

Nanofibrillated cellulose (NFC), produced from wood fibers via mechanical or chemical disintegration [34, 40], exhibits intriguing properties such as high surface area, high hydrogen bonding ability, and good mechanical strength [47, 51]. Recently, NFC-gel has been used to manufacture nearly transparent and smooth films [22, 28, 43]. We have found that precursor pulps with low negative charge used to produce NFC significantly reduces their impregnation with water and facilitates analyte penetration into the supporting material. This is likely due the small porosity and compact structure of respective NFC-films [33]. Therefore, water resistance ability should be imparted for NFC films to enter the field of diagnostic applications. Moreover, the surface chemistry of NFC-film needs to be adjusted to reduce non-specific adsorption [30].

TEMPO-mediated oxidation selectively converts the primary hydroxyls of cellulose to their carboxyl form, which can be further utilized in immunoassays [6, 11, 18,

39–41]. In fact, TEMPO-oxidized NFC-gel has been used as a starting material for highly transparent films with low air permeability [10]. Unfortunately, the high negative charge of TEMPO-oxidized NFC films results in rather low water resistance. However, surface specific post-oxidation of the novel, water resistant NFC-films could offer an alternative pathway to produce immunodiagnostic platforms with low porosity, high stability and suitable conjugation sites for immobilization of proteins. The dense and closed structure of NFC-films reduces diffusion of water which in turn diminishes the oxidation reaction inside the film's structure and thus increases its water resistance [43].

The use of inkjet printing in biosensors and immunoassays supported on paper and other substrates has been widely reported [1, 8, 17, 24]. The main advantages of the inkjet printing technique include small demand of printing liquids (expensive purified antibodies and enzymes can be used) [7], and the lack of physical contact with the object, which reduces the risk for surface contamination. Moreover, typical small droplet sizes (in the scale of picoliters), allow control of the surface concentration of sensing molecules, and the topology of deposition of sensing molecules at the support's surface-analyte fluid interface [38].

In this paper we describe a method for topological modification of water resistant NFC films using TEMPO-oxidation. NFC-films were first TEMPO-oxidized to introduce carboxyl groups on their surface. Next, carboxyl groups were converted to amine-reactive via EDC/NHS coupling chemistry (see Scheme 1). Subsequently, the conjugation of antibodies and proteins on activated NFC-films were demonstrated by inkjet printing and physical adsorption of polyclonal antihuman IgG and bovine serum albumin (BSA). The chemical and topological changes of the NFC-films were investigated by using quartz crystal microbalance with dissipation (QCM-D), contact angle measurements, X-ray photoelectron spectroscopy (XPS), confocal laser scanning microscopy (CLSM), atomic force microscopy (AFM) and conductometric titration techniques.

2 Experimental Section

2.1 Materials

Antihuman IgG (#I9764), human IgG (#I4506), NHS (*N*-hydroxysuccinimide, #130672), EDC (1-ethyl-3-[3-dimethylaminopropyl]carbodiimide hydrochloride, #03450), ethanolamine (#398136), BSA (bovine serum albumin, #A7030), dansyl chloride (#39220), FITC (Fluorescein 5(6)-isothiocyanate, #46950), and TEMPO free radical [(2,2,6,6-tetramethyl-piperidin-1-yl)oxyl, #426369] were obtained from Sigma-Aldrich (Helsinki, Finland). The water used in all experiments was deionized and further purified with a Millipore Synergy UV unit (MilliQ-water). All other chemicals were used without any purification steps. An Epson R800 piezoelectric inkjet printer with a CD-printing tray was used without any modifications. Clean unused inkjet cartridges were obtained from MIS Associates, MI, USA.

2.2 Methods

2.2.1 *Preparation of Nanofibrillar Cellulose (NFC) Films and NFC Model Surfaces*

The NFC films used in this work were prepared as described elsewhere [33]. In brief, bleached hardwood pulp (birch) was mechanically processed using a Masuko grinder with five passes and then further disintegrated by a M110P fluidizer (Microfluidics corp., Newton, MA, USA) with six passes. The produced NFC-gel was then filtered to remove the excess of water with a filter membrane using 2.5 bar. The film was then rolled five times with a smooth metal rolling pin to further consolidate the structure of the film. Finally the prepared films were dried between clean blotting boards (highly absorbent paper sheets) under external pressing and stored under ambient conditions until used.

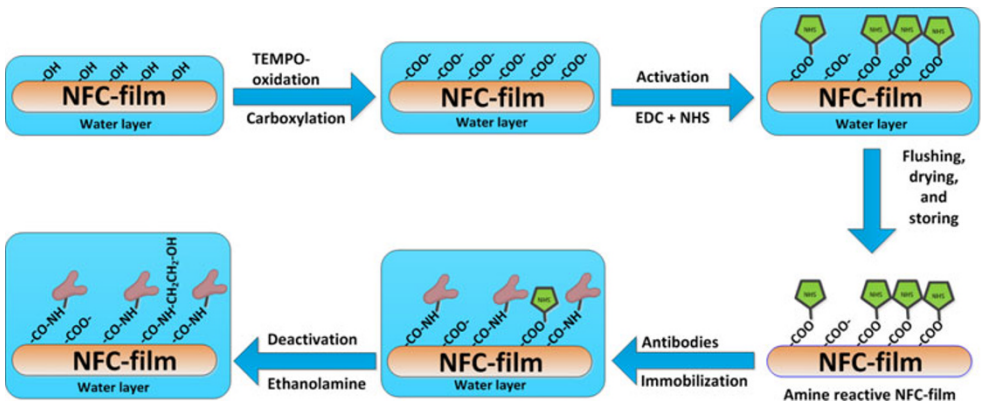

Scheme 1 Schematic illustration of the topological modification of NFC-film using sequential TEMPO-mediated oxidation and EDC/NHS activation. Antibodies can be immobilized on the activated NFC-films by either inkjet printing or physical adsorption

NFC model surfaces (thin films) were prepared as described by Ahola et al. [2]. In brief, bleached hardwood pulp (birch) was mechanically treated (five times with Masuko grinder) and then further disintegrated by microfluidization with 20 passes. The individual cellulose nanofibrils were then produced using mechanical stirring and tip ultrasonication (10 min, 25 % amplitude). The resulting NFC suspension was centrifuged at 10,400 rpm for 45 min and colloidal nanofibrils were then collected from the supernatant by pipetting. The collected nanofibrils (0.148 wt% NFC in water) were then spin-coated (Model WS-650SX-6NPP, Laurell Technologies, PA, USA) at 3,000 rpm and 90 s spinning time on QCM SiO_2-crystals carrying a thin layer of PEI. The NFC-coated QCM crystals were stored in a desiccator and prior to use in QCM-D measurements they were stabilized overnight in water.

2.2.2 *Activation of the NFC Films via TEMPO-Mediated Oxidation and EDC/NHS Treatment*

NFC-films were oxidized by using the 2,2,6,6,-tetramethylpipelidine-1-oxyl radical (TEMPO) NaBr–NaClO system as described by Isogai et al. [18]. 0.13 mmol TEMPO and 4.7 mmol NaBr were dissolved in 100 mL water. Then 5.65 mmol NaClO was added in the solution, and the pH was adjusted to 10 by adding 1 M HCl. Next, NFC-film (size 2.5 × 2.5 cm^2) was placed in a glass petri dish in which the prepared TEMPO-solution was added. NFC-films were kept in the solution for times varying from 10 to 300 s, and the oxidation reaction was quenched by adding ethanol and washing with a large amount of water to remove the excess of carboxylation chemicals. Finally, carboxylated NFC-films were made amine-reactive via EDC/NHS activation as follows: carboxylated NFC-film was kept in a solution of 0.1 M EDC and 0.4 M NHS (10 mM NAOAc buffer, pH 5) for 20 min, and then rinsed with water. Activated NFC-film was then dried between clean blotting boards to prevent film buckling.

2.2.3 *QCM-D In-situ Monitoring of TEMPO-Mediated Oxidation and EDC/NHS Activation of NFC Model Surfaces*

Interaction and analyses of the activation of the NFC thin films were carried out using a QCM-D E4 instrument (Biolin Scientific AB, Gothenburg, Sweden) with controlled flow [16, 36]. All measurements were performed using a constant 100 μL/min flow rate, 25 °C temperature, and all experiments were at least performed in duplicate. First, TEMPO-mediated oxidation reaction of NFC thin films was investigated by using QCM-D. To this end, TEMPO-solution (0.13 mmol TEMPO, 4.7 mmol NaBr, and 5.65 mmol NaOCl in water with fixed pH of 10) was allowed to flow over the QCM sensors carrying the NFC thin films for 2 min. The oxidation reaction was then quenched by adding ethanol in the oxidation solution (10 % v/v), and the constant flow was continued for 2 min to stop the carboxylation reaction. Next, the carboxylated NFC thin films were rinsed with water for 20 min to remove excess carboxylation chemicals. Finally, the surfaces were stabilized in 10 mM NaOAc buffer at pH 5. The carboxylated NFC surfaces were made amine reactive by flowing a solution of 0.1 M EDC with 0.4 M NHS (10 mM NaOAc buffer, pH 5) for 20 min. The excess of chemicals were then rinsed out with 10 mM NaOAc buffer. The activated amine NFC thin films were finally dried using a nitrogen gas, and stored in a desiccator, if not immediately used.

The measured shift in frequency obtained in QCM experiments was fitted to the Johannsmann's model [19] to quantify changes in mass of the QCM sensors carrying the NFC thin films. The iterative process in the model used the third, fifth, and seventh frequency overtones of the QCM-D crystal.

2.2.4 *Conjugation of BSA and Antihuman IgG on Activated NFC Surfaces Monitored In-situ by QCM-D*

The reactivity of activated NFC thin films was verified using QCM-D as follows. The pre-activated NFC surfaces were first stabilized in 10 mM NaOAc buffer at pH 5 for 1 h, and then 100 μg/mL of BSA solution (10 mM NaOAc buffer, pH 5) was introduced for 30 min. The pH conditions were selected, because BSA adsorption is maximized at its isoelectric point (pH 5). The conjugation was confirmed by a sequential rinsing sequence NaOAc buffer (pH 5), 10 mM NaCl (pH 10), and again with NaOAc buffer (pH 5). It should be noted that the rinsing with alkaline buffer (10 mM NaCl, pH 10) resulted in an electrostatic repulsion between BSA and the activated NFC substrate which in turn removed electrostatically bound BSA. Two reference experiments were performed identically by using unmodified and TEMPO-oxidized NFC surfaces; this was done in order to rule out the contribution of interactions between BSA and the substrate different than covalent bonding.

The conjugation of antihuman IgG on activated NFC surfaces was also verified using QCM-D by flowing 100 μg/mL of antihuman IgG solution (10 mM NaOAc, pH 5) for 30 min followed by buffer rinsing (10 mM NaOAc, pH 5). The excess of NHS-esters was then removed by rinsing with 0.1 M ethanolamine solution at pH 8.5 for 15 min. Non-specific binding of proteins was prevented by using a 15 min Superblock treatment. Superblock is a protein solution that fills the free spaces

between the antibodies, thus preventing the non-specific binding of antigens on the surface of biointerface. The detection sensitivity of prepared biointerfaces with conjugated antihuman IgG was verified by adsorbing 10 μg/mL hIgG solution (10 mM phosphate buffer, pH 7.4) for 10 min. As a reference NFC films without antihuman IgG were tested. In addition, two reference experiments were performed identically by adsorbing antihuman IgG and human IgG on unmodified and TEMPO-oxidized NFC surfaces; this was done in order to rule out the contribution of interactions between antihuman IgG and the substrate different than covalent bonding as well as to explore the non-specific binding of proteins.

2.2.5 *Inkjet Printing and Physical Adsorption of Antihuman IgG on Activated NFC-Films*

Inkjet printing of antibodies on activated NFC-films was demonstrated using EPSON R800 inkjet printer. Fluorescence (dansyl or FITC-probe)-stained antihuman IgG (1 mg/mL) in 10 mM phosphate buffer (pH 7.4) was printed on the activated NFC films (size 2 × 4 cm^2) using a CD printing tray with an EPSON print-CD software. The fluorescence staining of antihuman IgG was done following the procedures described elsewhere [37, 13]. Stained antibody solutions were purified with Amicon Ultra centrifugal filter tubes (Mw cutoff of 30 kD) using three cycles of 10 mM phosphate buffer (pH 7.4) and a total rinsing volume six times larger than the original sample volume. The stained antihuman IgG was diluted to the final concentration using 10 mM phosphate buffer (pH 7.4) followed by an immediate printing on activated NFC films. The printing conditions were selected using a CMYK color profile which allows printing from a selected cartridge. All other cartridges were filled with 10 mM phosphate buffer (pH 7.4). Printed NFC films were then treated with 0.1 M ethanolamine at pH 8.5 for 15 min, and dried at ambient conditions. The fluorescence of NFC films was investigated using UV-light (366 nm, Camag, Berlin, Germany), CLSM and AFM.

The physical adsorption of antihuman IgG on the activated NFC films was also examined. FITC-stained or unstained antihuman IgG (100 μg/mL) in 10 mM phosphate buffer (pH 7.4) was adsorbed on unmodified and activated NFC for 20 min. Corresponding films were then treated with 0.1 M ethanolamine at pH 8.5 for 15 min, rinsed with 10 mM phosphate buffer (pH 7.4), and 10 mM NaCl (pH 10) to remove electrostatically bound antibodies. Finally, the surfaces were rinsed with Milli-Q water and dried at ambient conditions. Adsorbed FITC-stained antihuman IgG on unmodified and activated NFC films was imaged using CLSM.

2.2.6 *Contact Angle Measurements*

Changes in the surface hydrophilicity of TEMPO-oxidized NFC films were monitored using a contact angle goniometer CAM 200 (KSV instruments Ltd, Helsinki, Finland). Measurements were performed at room temperature with water as a probe liquid. A droplet volume of 6.5 μL and a recording time of 120 s were used to measure the time dependency of the contact angle. Contact angles were measured on three different locations on each sample.

2.2.7 *Conductometric Titration*

The increase in negatively charged groups (carboxyls) in TEMPO-oxidized NFC-films was measured using a conductometric titrator 751 GPD Titrino (Metrohm AG, Herisau, Switzerland) following SCAN-CM 65:02 standard method. NFC-films (size 2.5 × 2.5 cm^2) were acid washed with 0.01 M HCl for 1 h, and then disintegrated in water with a blade type homogenizer Polytron PT 2000 (Kinematica Inc., NY, USA). The conductometric titration was performed by adding 0.02 mL of 0.1 M NaOH using 30 s intervals. The amount of weak acid (carboxyl) groups was calculated as described in the standard method (SCAN-CM 65:02).

2.2.8 *X-Ray Photoelectron Spectroscopy*

The surface chemistry of the topmost 10 nm of the NFC films was examined using a Kratos Analytical AXIS 165 electron spectrometer with a monochromatic Al Kα X-ray source at 100 W and a neutralizer. The XPS experiments were performed on the dry films, which were pre-evacuated overnight. At least three different spots of each sample were scanned. Spectra were collected at an electron take-off angle of 90° from sample areas less than 1 mm in diameter. Elemental surface compositions were determined from low-resolution measurements (80 eV pass energy and 1 eV step), while the surface chemistry was probed with high resolution measurements (20 eV pass energy and 0.1 eV step). The carbon C1s high-resolution spectra were curve fitted using parameters defined for cellulosic materials [20] and all binding energies were referenced to the aliphatic carbon component of the C1s signal at 285.0 eV [3]. According to the in situ reference (100 % cellulose ash free filter paper), measured along with each sample batch, the conditions in UHV remained satisfactory during the XPS experiments [20].

2.2.9 *Macroscale and Nanoscale Topography: CLSM and AFM*

The macro-scale topography of NFC films was analyzed with a Leica TCS SP2 CLSM (Leica microsystems CMS

GmbH, Manheim, Germany). The image was obtained using a reflection image mode with an excitation wavelength of 488 nm and a detection wavelength range of 490–550 nm. The image size was 750 × 750 μm^2. The intensity images were scanned using an averaging mode and constant imaging conditions (laser power was 848 V in all measurements). Intensity of the fluorescence images was measured using analysis tool of Photoshop (Adobe). The intensity was measured from the unmodified raw images. 3D-image was obtained from 60 optical sections of the NFC film by using topography. No sample pretreatment was done except placing the sample between two clean microscopy glasses. The roughness profiles of the NFC films were calculated using the obtained topological 3-D image together with Leica confocal microscope software.

Nano-scale topological changes on the NFC films were investigated using Nanoscope IIIa Multimode scanning probe microscope (Digital Instruments, Inc., Santa Barbara, CA). The images were scanned using the silicon cantilevers (Ultrasharp μmasch, Tallinn, Estonia). At least three different locations on each sample were scanned with image sizes of 5 × 5 and 1 × 1 μm^2. No image processing was done except image flattening. Roughness profiles were calculated using 5 × 5 μm^2 images.

3 Results and Discussion

3.1 Carboxylation of NFC-Films

The water resistance of unmodified NFC-films was investigated by experiments in which the films were immersed in water for several days accompanied by frequent treatments with ultrasonic energy. Interestingly, the films remained rather intact suggesting that films of low-charged NFC prepared by pressure filtering have adequate wet strength properties [33]. The water resistance of the films is probably improved by virtue of lower porosity and increased hydrogen bonding which both reduce the water intake. In comparison, the water resistance of the free standing NFC films is rather poor. The macroscale topography of the unmodified NFC film was characterized by CLSM (Fig. 1a). The wire markings from the filtration membrane are clearly visible but no macroscale voids or pores were observed, suggesting a rather uniform NFC film surface with RMS roughness of about 6.8 ± 1.0 μm. The improved water resistance is expected to diminish the diffusion of biomolecules into the NFC film, thus enhancing the specificity of the immunoassay.

Unmodified NFC-films were carboxylated via TEMPO-mediated oxidation. The substantial increase of carboxyl groups on the surface of TEMPO-oxidized NFC-films was verified by conductometric and contact angle measurements (Fig. 2). It should be noted that the contact angle of unmodified NFC-film was 44°, i.e., similar to the values reported elsewhere [43]. However, after 10 s oxidation, the contact angle was reduced to 19°, indicating a rather hydrophilic surface after such a short oxidation time. Furthermore, prolonged oxidation (over 30 s) was found to further increase the hydrophilicity of the film surfaces as contact angle values well below the detection limit of 15° were measured. This demonstrates the fast reaction kinetics of TEMPO-oxidation which allows for rapid carboxylation of NFC. Contact angles of the carboxylated NFC films were even lower than the values reported for films prepared from TEMPO-oxidized cellulose nanofibrils (pre-oxidation) [10]. Possible explanations might be the high surface carboxyl content of oxidized NFC films as well as concurrent peeling off reaction that has been found to occur during TEMPO-oxidation [14]. This reaction can open the structure of cellulose microfibrils and therefore increase the specific surface area. It is important to note here that the XPS measurements did not reveal residual oxidation chemicals, i.e., the observed hydrophilicity is not deriving from the residual reagents or unreacted chemicals.

The changes in total charge as a function of TEMPO-oxidation were followed by conductometric titration (Fig. 2). The charge of the unmodified NFC film was 72 μeq/g (reference), most likely due to the presence of hemicelluloses in the hardwood fibers used for NFC production [34]. The charge increased more than two-fold (169 μeq/g) after a 30 s oxidation period. The highest charge was found after 5 min oxidation (237 μeq/g). This level of charge was significantly lower than that observed upon TEMPO-oxidation of suspended nanofibrils (charge 1,500 μeq/g) [41], thus strongly suggesting that the carboxylation mainly occurred on the surface of the NFC film. It should be noted that the aldehyde content of NFC film was not measured since only the carboxyl groups were utilized for the following EDC/NHS coupling reaction [13]. The water resistance of TEMPO-oxidized NFC-films was tested by immersing them in water for several hours. The films remained intact thus suggesting that the carboxyl formation likely occurred only on the surface of a NFC-film because the oxidation inside the film would result in swelling and subsequent disintegration of the film.

3.2 EDC/NHS Activation of TEMPO-Oxidized NFC Films

The activation of the TEMPO-oxidized NFC was verified by using thin NFC films pre-adsorbed on sensors for in situ QCM-D monitoring. It is important to note that the data range on frequency shift axes in QCM isotherms is the negative change in frequency, which increases with mass gain (due to adsorption or water coupling). NFC model

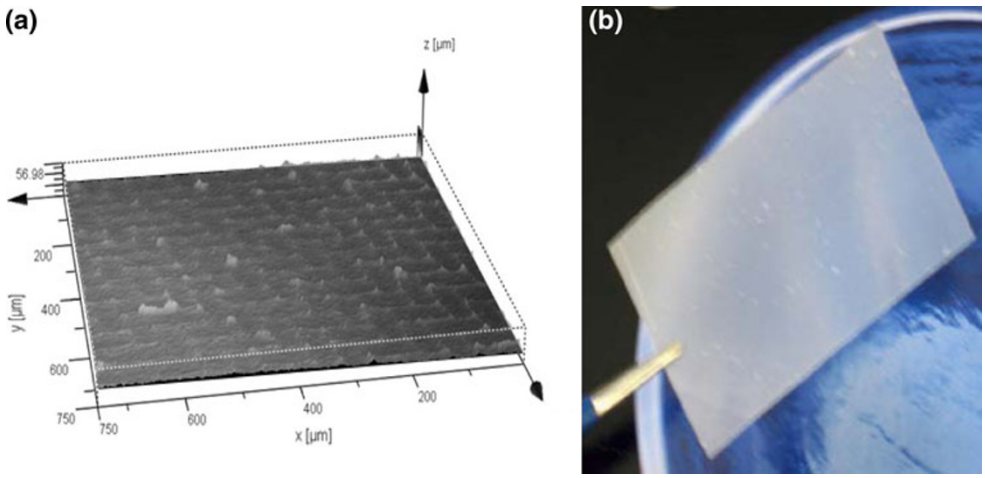

Fig. 1 Confocal laser scanning microscopy (CLSM) image of unmodified NFC film (**a**). The reflection mode with topological imaging mode was used. Digital photograph (4.5 × 2.5 cm^2) of an unmodified NFC film (**b**)

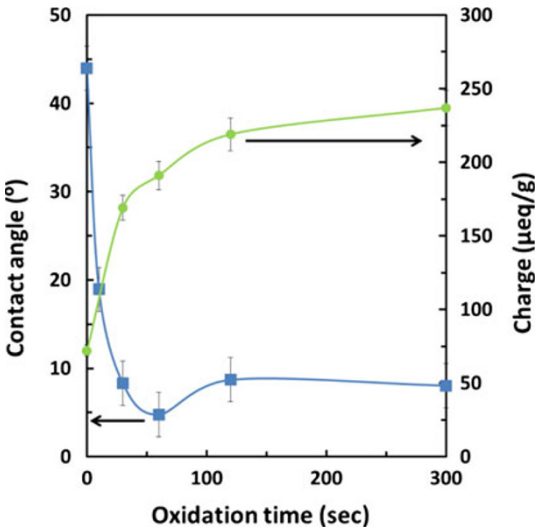

Fig. 2 The effect of TEMPO-mediated oxidation on contact angle (*blue line*) and total charge (*green line*) of NFC films as a function of the oxidation time. Contact angles were obtained after 10 s recording. The *lines* are not fitted, but just added as aid to the eyes. Spreading out of the water droplet was noted to occur at contact angles below 15°

surfaces were first carboxylated for 2 min with a solution containing the TEMPO-oxidation reagents. This treatment resulted in an instant negative frequency shift which is likely related to the formation of carboxyl groups with increased amount of coupled water (Fig. 3a). It should be indicated that a drastic increase in energy dissipation occurred, as recorded simultaneously in the QCM dissipation signal (data not shown). Altogether, there is an indication of a buildup of large amounts of hydration water after TEMPO treatment of the NFC film. As expected, water rinsing further decreased the frequency shift (from −75 to −130 Hz) and increased the dissipation values (35×10^{-6}). This indicates that the removal of electrolytes and other chemical increased the total charge of the system which in turn promoted further swelling of the NFC film. The mass of the coupled water after TEMPO-oxidation and water rinsing was found to be 25.3 mg/m^2 (calculated using Johannsmann's model), which corresponds to a thickness change of ca. 25 nm assuming the water layer is on a flat surface. However, the addition of 10 mM sodium acetate buffer (pH 5) reduced the swelling of the NFC film, as observed as an increase in the frequency shift. The EDC/NHS treatment of carboxylated NFC thin film decreased both the frequency (change over −25 Hz after buffer rinsing) and dissipation. This demonstrates the formation of NHS-esters and also the concurrent decrease in anionic charge, which reduces the swelling of the NFC thin film. Furthermore, after buffer rinsing the frequency and dissipation quickly reached plateau levels, indicating a level-off in NHS-ester formation. It should be noted that no desorption of NHS-esters was observed during the extended rinsing period. At the end of NHS conjugation, the activated NFC film was dried with nitrogen gas and stored overnight in a desiccator prior to reactivity tests with BSA (Fig. 3b).

TEMPO-oxidized and EDC/NHS activated NFC-films were also analyzed using XPS. While the carboxylation of the NFC films could not be followed via XPS measurements (as reported by us and other groups [9], most probably due to the medium-dependent surface reconstruction of cellulose in dry medium [21], the EDC/NHS activation of the carboxyl groups leads to ester groups, which are XPS detectable [21, 48]. Furthermore, the NHS-esters formed during film activation contain nitrogen not otherwise present in unmodified or carboxylated films. Therefore, nitrogen signal was used as a fingerprint in XPS measurements. The XPS spectra in Fig. 4 show that all the studied surfaces were clean and have characteristic features of pure cellulose. Even the significant non-cellulosic C–C component in the unmodified and carboxylated films is in good accordance with other reports [21]. Importantly, the

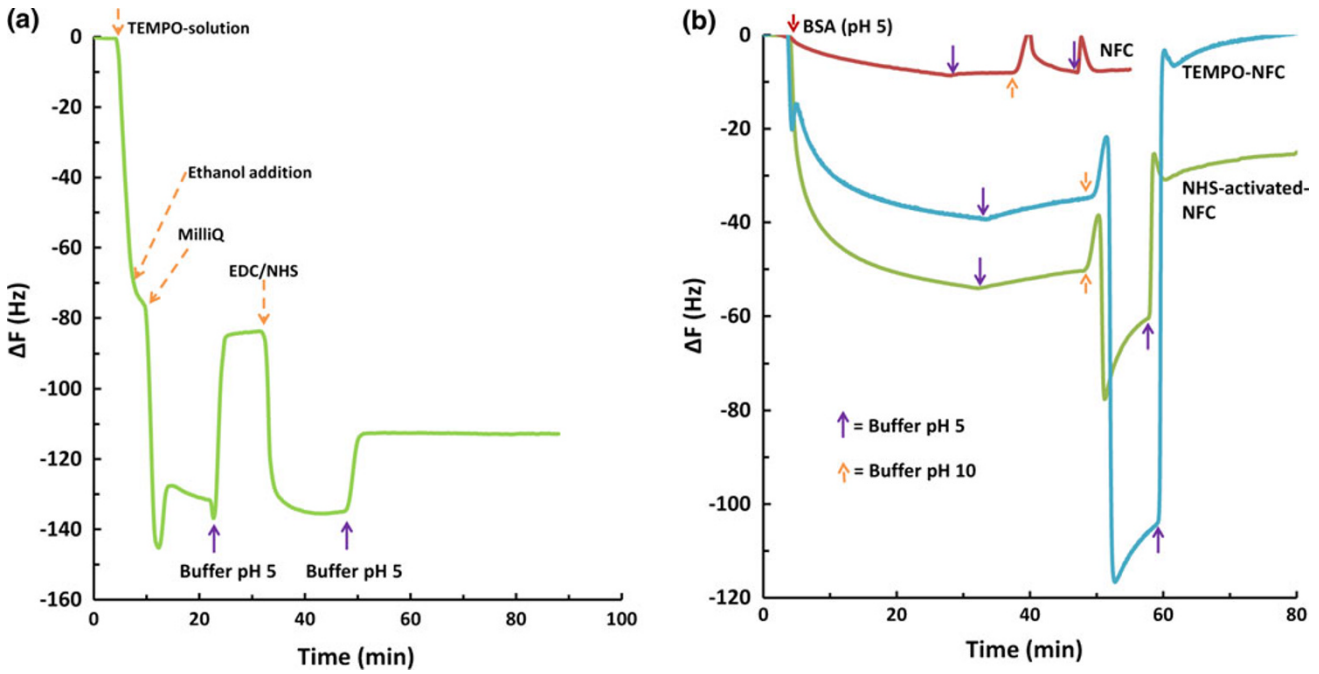

Fig. 3 QCM-D data of sequential TEMPO-oxidation and EDC/NHS activation of a NFC-surface (**a**). Adsorption of 100 μg/mL BSA in 10 mM NaOAc (pH 5) on unmodified NFC, TEMPO-oxidized NFC and EDC/NHS activated TEMPO-oxidized NFC (**b**). EDC/NHS activated NFC-films was dried in a desiccator overnight before the adsorption experiments. Adsorption data was obtained using fifth normalized overtones

EDC/NHS activation resulted in a clear nitrogen signal (red line in Fig. 4), accompanied by a similar increase in the C1s carbonyl component (Fig. 4 and Supporting information Table 1). This indicates that the NHS-esters were formed on the surface of the NFC film.

The nanoscale topological changes of NFC-films (images of 1 × 1 μm^2) were characterized by AFM (Fig. 5a–c). In addition, images of 5 × 5 μm^2 are shown in the Fig. S2. Clusters of cellulose nanofibrils were clearly observed in the unmodified NFC film. No large voids or pores were observed, which indicates that the natural affinity between cellulose fibrils leads to a formation of rather evenly distributed film. The roughness of unmodified NFC film was found to be approximately 35.4 nm. After TEMPO-oxidation of NFC film the fibrillar structure seemed to be covered by a gel-like layer (Fig. 5b) which can be observed as an increased phase difference (Fig. S1) and indicates the softening of the surface. The formation of gel-like structure was probably triggered by carboxylated cellulose nanofibrils, which bind significant amount of water (see QCM-D data Fig. 3a). The roughness of the TEMPO-oxidized NFC-film was found to be approximately 44.5 nm (Fig. 5c). EDC/NHS activation removes the charge of the NFC film reducing the water binding capacity, as can be observed in Fig. S2c, where the surface is similar compared to that of the unmodified NFC film. The roughness of EDC/NHS activated NFC film was found to be approximately 49.6 nm. We also used CLSM to investigate the topological changes in TEMPO-oxidized and EDC/NHS activated NFC films. However, we did not observe major changes compared to that of unmodified NFC-film. This was likely due to the detection limit of the CLSM technique (detection limit of CLSM is approximately 200 nm).

3.3 Amine Reactivity of EDC/NHS Activated NFC Films

We used QCM-D in situ monitoring to investigate the reactivity of EDC/NHS activated NFC films. In order to demonstrate the amine reactivity, BSA was used as a weight marker easily detectable in QCM-D. BSA (100 μg/mL) was adsorbed at pH 5 on unmodified, TEMPO-oxidized and NHS-activated NFC films and the resulting surfaces were sequentially rinsed with NaOAc (pH 5), 10 mM NaCl (pH 10) and NaOAc (pH 5) buffer solutions (Fig. 3b). The control experiment with unmodified NFC-surface revealed irreversible binding of BSA as can be observed by negative frequency shift (−8 Hz, 1.6 mg/m^2). This is not totally surprising since at the isoelectric point (pI = 5) a rather large amount of BSA has been found to adsorb on cellulose surfaces [31]. In addition, similar results for the adsorption of BSA on non-cellulosic surfaces have been observed as a result of reduced solvency at the pI [25, 46]. However, it should be noted that alkaline buffer (10 mM NaCl, pH 10) rinsing did not remove the bound BSA as would have been expected from the electrostatic

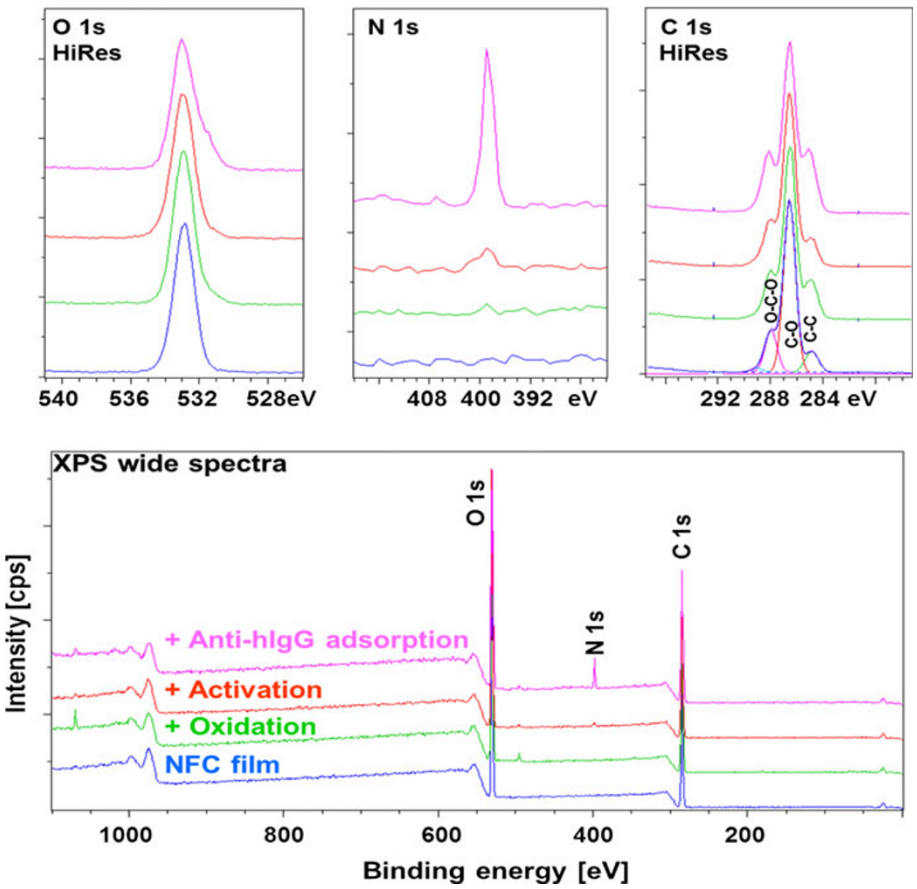

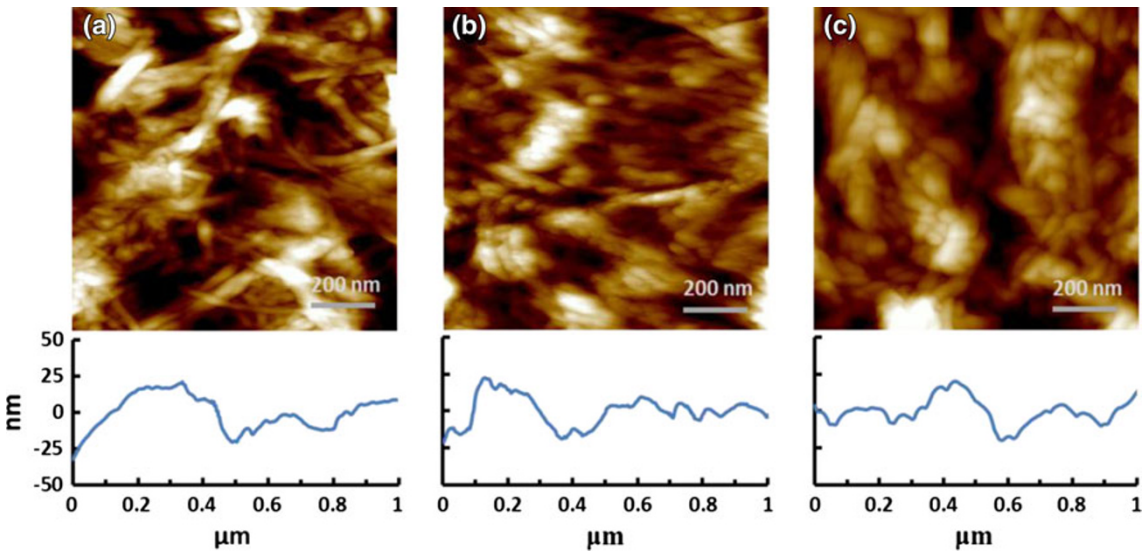

Fig. 4 XPS spectra of unmodified NFC, TEMPO-oxidized NFC, EDC/NHS activated TEMPO-oxidized NFC and EDC/NHS activated TEMPO-oxidized NFC with immobilized antihuman IgG

Fig. 5 AFM images in air of an unmodified NFC film (**a**), and films after TEMPO oxidation (**b**) followed by EDC/NHS activation (**c**). TEMPO-oxidation time was 120 s

repulsion between negatively charged BSA and NFC surfaces. One possible explanation is the lower negative charge of unmodified NFC which decreases its interaction with water and therefore the irreversible adsorption of proteins may be enhanced [29].

Adsorption of BSA on TEMPO-oxidized NFC film was found to be significantly higher (−35 Hz, 6.8 mg/m^2) than that on the unmodified NFC. However, the binding of BSA was reversible as the alkaline buffer (10 mM NaCl, pH 10) rinsing completely removed the bound protein. This is

likely due to the electrostatic repulsion between the negatively charged BSA (pI = 5) [4] and negatively charged carboxylated TEMPO-oxidized NFC thin films (pI of carboxyls approximately 4.5) [15]. Furthermore, this demonstrates the regenerability of the carboxylated NFC surface. It should be mentioned that the adsorption of BSA on TEMPO-oxidized NFC thin film was also investigated at pH 7.4 and no adsorption was observed, because of electrostatic repulsions (data not shown). The initial adsorption of BSA on EDC/NHS activated NFC thin films was found to be higher (−50 Hz, 9.8 mg/m^2) than those on unmodified and TEMPO-oxidized NFC surfaces. This can be explained by the EDC/NHS-activation of free carboxyls which in turn reduces the negative charge of the NFC, thus decreasing the surface hydrophilicity, which is known to be beneficial for protein adsorption [27]. It can be observed from Fig. 3b that even after alkaline buffer (10 mM NaCl, pH 10) rinsing approximately half (−25 Hz, 4.9 mg/m^2) of the initially adsorbed BSA remains on the NFC thin film. This is most likely due to the hydrolysis of NHS-esters in alkaline conditions which in turn increases the negative charge of the activated NFC-surface [13, 45]. Moreover, the restored anionic charge results in an electrostatic repulsion with negatively charged BSA leading to a removal of electrostatically bound protein. This clearly demonstrates that the EDC/NHS activation of TEMPO-oxidized NFC can be used to produce a reactive platform, which allows for the covalent conjugation of amine-bearing biomolecules.

3.4 Immobilization of Antibodies on EDC/NHS Activated NFC Films

The attachment of antibodies was investigated by using a chemical adsorption of FITC-stained molecules on the activated NFC films (Fig. 6). The fluorescence imaging was carried out using laser wavelength 488 nm, where fluorescein produces an emission approximately at a wavelength of 520 nm. It should be mentioned that no auto-fluorescence of activated NFC was observed. FTIC-stained antihuman IgG (100 μg/mL) was adsorbed on the unmodified NFC-film and activated NFC-film. The surfaces were then treated with ethanolamine and 10 mM NaCl (pH 10) to remove the excess of NHS-groups as well as electrostatically bound antibodies. The adsorbed amount of antihuman IgG on unmodified NFC film was found to be rather low, which can be observed as a weak fluorescence emission (intensity approximately 1.8). As expected, the adsorption of antihuman IgG on activated NFC surfaces was significantly higher (intensity approximately 18.76). Furthermore, electrostatically bound antihuman IgG was removed from unmodified NFC film upon alkaline (pH 10) washing, whereas the fluorescence remained in EDC/NHS activated NFC film after such a treatment. It should be noted that the lattice type marking on the fluorescence image (Fig. 6b), originates from the screen used as support during the process of the NFC film manufacture. Immobilization of antihuman IgG on the surface of activated NFC-films was also verified by XPS using nitrogen as a fingerprint for protein (Fig. 4). A clear increase in the nitrogen content (up to 6 wt%, Supporting Information Table 1) confirms the presence of antibody (Fig. 4).

3.5 Biological Activity of the Immobilized Antihuman IgG

In situ QCM-D monitoring was used to explore the conjugation reaction of antihuman IgG on EDC/NHS activated NFC-surface as well as the subsequent adsorption of hIgG (see Fig. 7). NFC thin films were first TEMPO-oxidized and EDC/NHS activated as described earlier. Next, a solution of antihuman IgG (100 μg/mL) was adsorbed on the activated NFC surface followed by rinsing with given buffer solution. The initial adsorbed amount of antihuman IgG after buffer rinsing was found to be approximately −90 Hz (18 mg/m^2). However, the addition of ethanolamine (pH 8.5) significantly decreased the adsorbed amount to −23 Hz (4.6 mg/m^2) representing the amount of conjugated anti-body. It is important to note here that the ethanolamine treatment converts unused activated carboxyls to corresponding ethylamides, which are somewhat hydrophobic. Therefore, it is possible that the observed increase in the QCM-D frequency (decrease in the adsorbed amount) is at least partially caused by the decrease in the coupled water on the NFC-surface. Moreover, the increase in the hydrophobicity may reduce the specificity of the biointerface due to the hydrophobic–hydrophobic interactions between the surface and proteins, but it was prevented by adsorbing a blocking agent (superblock) before antigen detection. After an ethanol amine treatment, the NFC surface was treated with superblock blocking agent to reduce the adsorption of positively charged hIgG (pI about 8) [12] on the anionic NFC surface. Human IgG (100 μg/mL) was adsorbed on the antihuman IgG interface at pH 7.4 and the adsorbed amount was found to be −5 Hz (0.93 mg/m^2). As a reference, and to demonstrate the amount of non-specific binding, human IgG was adsorbed on ethanolamine treated EDC/NHS activated NFC surface. As can be observed from Fig. S3 the adsorbed amount of human IgG on the reference surface is significantly lower than that of the antihuman IgG containing surface. This clearly demonstrates that the developed NFC-antihuman IgG interface can be used for capturing the human IgG from a solution. Moreover, the negligible non-specific adsorption of human IgG on NFC surface after the superblock treatment allows the use of NFC films in

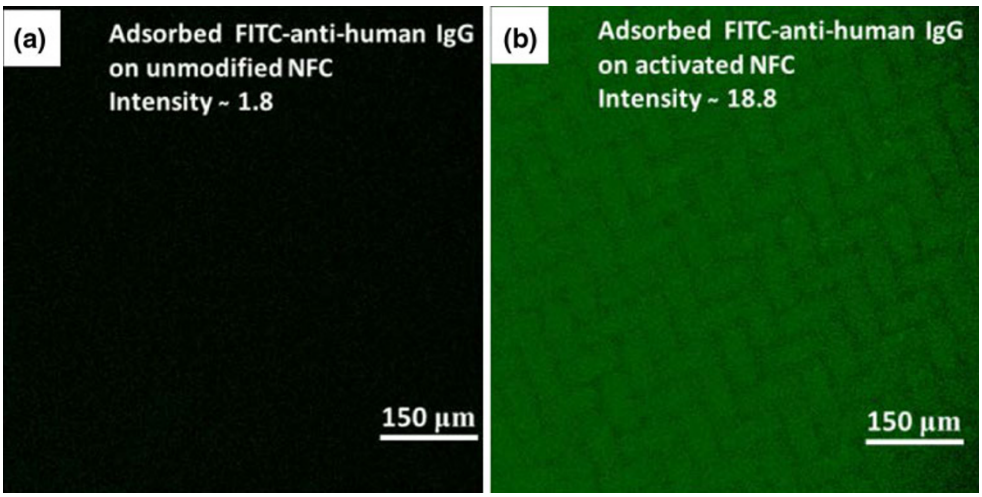

Fig. 6 CLSM intensity images of adsorbed FITC-stained antihuman IgG (100 µg/mL) in 10 mM phosphate buffer (pH 7.4) on unmodified NFC film (**a**) and EDC/NHS activated NFC-film (**b**). Both films were rinsed with 10 mM NaCl (pH 10) to remove electrostatically bound antibodies. Images are recorded using 848 V laser with constant imaging conditions

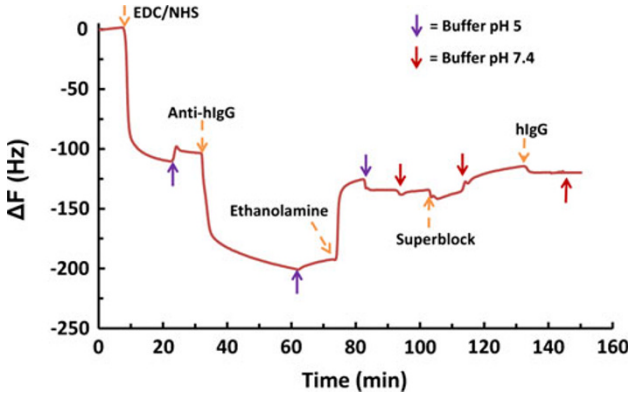

Fig. 7 QCM-D data of the adsorption of human IgG (hIgG) on EDC/NHS activated NFC-film in the presence of conjugated antihuman IgG. Conjugation of IgG resulted in a small shift in frequency

immunoassays, where positively charged target molecules are monitored. The amount of immobilized antihuman IgG on activated NFC-film was found to be similar to those reported in the literature [5, 32]. It should also be mentioned that the adsorbed amount of human IgG on the antihuman IgG interface was over twofold when compared to published results with anti-hIL-1ra conjugation on CMC-PEI hydrogel [5].

3.6 Inkjet-Printing of Antibodies on EDC/NHS Activated NFC Films

Here we demonstrate the large scale and fast attachment of antihuman IgG on activated NFC films using inkjet-printing of dansyl-stained antihuman IgG (1 mg/mL, pH 7.4) on solid supports consisting of activated NFC films (see Fig. 8a). The film was rinsed with ethanolamine to remove the excess of NHS-groups, and also the majority of electrostatically bound antibodies (Fig. 7). After drying, fluorescence was detected under the UV-light (366 nm) radiation. It was observed that NFC film presented a significant auto-fluorescence. Yet, the texture of printed antihuman IgG was clearly visible and therefore indicated that the antibodies were irreversibly attached on the activated NFC film. The inkjet printing of antihuman IgG on the activated NFC film was further investigated using FITC-staining and CLSM. After printing the antihuman IgG texture on activated NFC film, the surface was rinsed with ethanolamine and 10 mM NaCl (pH 10) to remove non-covalently bound antibodies. Because of the higher magnification of CLSM only a border of the printed texture can be observed (Fig. 8b). In addition, AFM was used to explore topological changes on the NFC film containing antihuman IgG (Fig. 8c). The AFM images indicated that the antibody was covering the fibrillar structure of cellulose, and thus pointed towards a uniform printed layer. Moreover, RMS roughness of the image was approximately 25 nm which is lower compared to that of unmodified NFC films (35 nm). It is expected that the generic and sustainable nature of the proposed biointerface will open new venues for immobilizing antibodies and other functionalities of NFC films, which can be used as platforms for rapid diagnostic applications.

4 Conclusions

We demonstrate the use of activated NFC films as solid support for diagnostic applications. Surface activation (carboxylation and EDC/NHS coupling chemistry) was used to produce robust nanocellulose-based biointerfaces with hydrophilicity and not known toxicity properties suitable for antibody conjugation. Carboxylation enhanced the water resistance of the NFC-film, while the increased

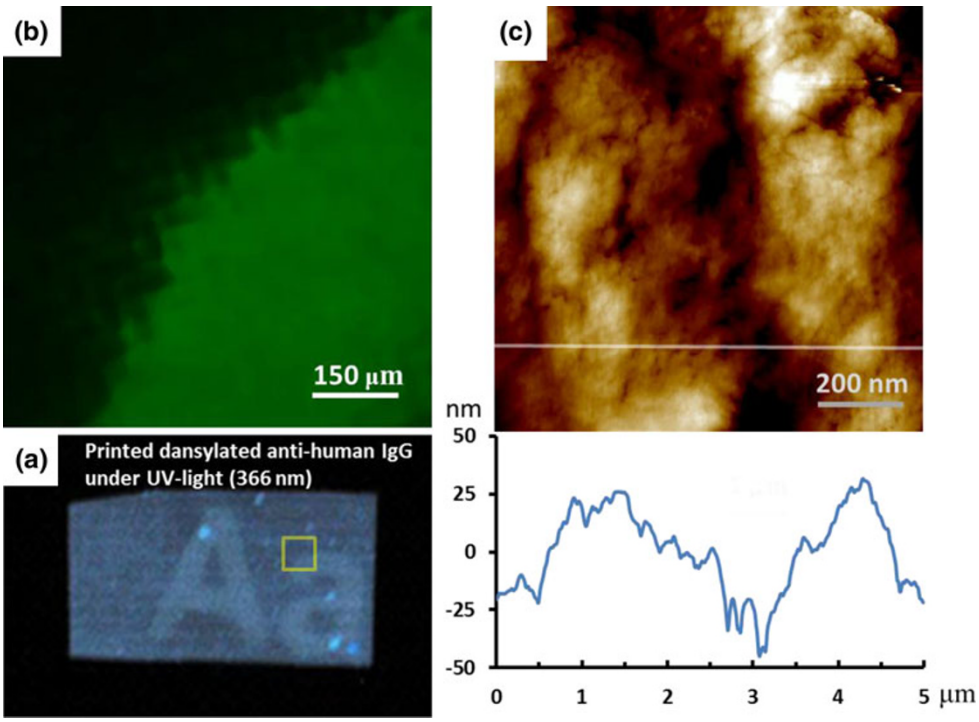

Fig. 8 Printed dansylated antihuman IgG (1 mg/mL in 10 mM phosphate buffer, pH 7.4) on EDC/NHS activated NFC film under UV-light (366 nm) (**a**). CLSM intensity image of printed FITC-stained antihuman IgG (1 mg/mL in 10 mM phosphate buffer, pH 7.4) on activated NFC film (**b**). Images recorded using 848 V laser. AFM height image on printed antihuman IgG on EDC/NHS activated NFC film (**c**). The *z*-scale of the image is 50 nm

hydrophilicity results in low non-specific binding, which is a requirement for affinity detection of biomolecules. Moreover, the developed NFC-based biointerfaces can detect positively charged molecules, which in many cases is challenging. Finally, it is demonstrated that inkjet printing can be used for the installation of antihuman IgG on activated NFC biointerfaces. Overall, the proposed platform based on chemical conjugation of antibodies on NFC after mild reaction conditions is expected to open new venues for the development of diagnostic applications based on inexpensive and sustainable materials.

Acknowledgments The Authors thank Ms. Anu Anttila for performing contact angle measurements and Ms. Aila Rahkola for performing conductometric titration measurements. Dr. Joseph Campbell is acknowledged for performing the XPS measurements. Ms. Ritva Kivelä is acknowledged for the technical assistance in AFM-imaging and M.Sc. Karoliina Junka for the assistance in conductometric titration of NFC.

Open Access This article is distributed under the terms of the Creative Commons Attribution License which permits any use, distribution, and reproduction in any medium, provided the original author(s) and the source are credited.

References

1. Abe K, Suzuki K, Citterio D (2008) Anal Chem 80(18):6928–6934
2. Ahola S, Myllytie P, Österberg M, Teerinen T, Laine J (2008) Bioresources 3(4):1315–1328
3. Beamson G, Briggs D (1992) High resolution XPS of organic polymers. Wiley, Chichester
4. Böhme U, Scheler U (2007) Chem Phys Lett 435(4–6):342–345
5. Carrigan SD, Scott G, Tabrizian M (2005) Langmuir 21(13):5966–5973
6. de Nooy A, Besemer AC, van Bekkum H (1995) Carbohydr Res 269(1):89–98
7. Delaney JT, Smith PJ, Schubert US (2009) Soft Matter 5(24):4866–4877
8. di Risio S, Yan N (2010) J Adhes Sci Technol 24:661–684
9. Diflavio J, Pelton R, Leduc M, Champ S, Essig M, Frechen T (2007) Cellulose 14(3):257–268
10. Fukuzumi H, Saito T, Iwata T, Kumamoto Y, Isogai A (2009) Biomacromolecules 10(1):162–165
11. Habibi Y, Chanzy H, Vignon M (2006) Cellulose 13(6):679–687
12. Hamilton R (1987) Clin Chem 33:1070–1075
13. Hermanson GT (2008) Bioconjugate techniques. Academic Press, San Diego
14. Hirota M, Furihata K, Saito T, Kawada T, Isogai A (2010) Angew Chem 122(42):7836–7838
15. Hoogendam CW, de Keizer A, Cohenstuart MA, Bijsterbosch BH, Smit JAM, Van Dijk JAPP, Van Derhorst PM, Batelaan JG (1998) Macromolecules 31(18):6297–6309
16. Höök F, Rodahl M, Brzezinski P, Kasemo B (1998) Langmuir 14(4):729–734
17. Hossain SM, Luckham RE, Smith AM, Lebert JM, Davies LM, Pelton RH, Filipe CD, Brennan JD (2009) Anal Chem 81(13):5474–5483
18. Isogai A, Kato Y (1998) Cellulose 5(5):153–164
19. Johannsmann D, Mathauer K, Wegner G, Knoll W (1992) Phys Rev B 46(12):7808–7815
20. Johansson L, Campbell JM (2004) Surf Interface Anal 36(8):1018–1022
21. Johansson L, Tammelin T, Campbell JM, Setala H, Osterberg M (2011) Soft Matter 7(22):10917–10924
22. Karabulut E, Wagberg L (2011) Soft Matter 7(7):3467–3474
23. Lequin RM (2005) Clin Chem 51(12):2415–2418

24. Lonini L, Accoto D, Petroni S, Guglielmelli E (2008) J Biochem Biophys Methods 70(6):1180–1184
25. Malmsten M, Emoto K, van Alstine JM (1998) J Colloid Interface Sci 202(2):507–517
26. Mansfield MA (2005) The use of nitrocellulose membranes in lateral-flow assays. In: Wong RC, Tse HY (eds) Drugs of abuse. Humana Press, New Jersey, pp 71–85
27. Martin M (1998) J Colloid Interface Sci 207(2):186–199
28. Nogi M, Iwamoto S, Nakagaito AN, Yano H (2009) Adv Mater 21(16):1595–1598
29. Norde W (2008) Colloids Surf B 61(1):1–8
30. Norde W (1996) Macromol Symp 103(1):5–18
31. Orelma H, Filpponen I, Johansson L, Laine J, Rojas OJ (2011) Biomacromolecules 12(12):4311–4318
32. Orelma H, Teerinen T, Johansson L, Holappa S, Laine J (2012) Biomacromolecules 13(4):1051–1058
33. Österberg M, Ly T, Vartiainen J, Laine J (2012) Strong nanofibrillated cellulose films with high barrier properties. 8th International Paper and Coating Chemistry Symposium 2012, p 234–236
34. Pääkkö M, Ankerfors M, Kosonen H, Nykänen A, Ahola S, Österberg M, Ruokolainen J, Laine J, Larsson PT, Ikkala O, Lindström T (2007) Biomacromolecules 8(6):1934–1941
35. Pelton R (2009) Trends Anal Chem 28(8):925–942
36. Rodahl M, Hook F, Krozer A, Brzezinski P, Kasemo B (1995) Rev Sci Instrum 66(7):3924–3931
37. Ronald B (2001) J Pharmacol Toxicol Methods 45(3):247–253
38. Rose D (1999) Drug Discov Today 4(9):411–419
39. Saito T, Isogai A (2004) Biomacromolecules 5(5):1983–1989
40. Saito T, Kimura S, Nishiyama Y, Isogai A (2007) Biomacromolecules 8(8):2485–2491
41. Saito T, Nishiyama Y, Putaux J, Vignon M, Isogai A (2006) Biomacromolecules 7(6):1687–1691
42. Siró I, Plackett D (2010) Cellulose 17(3):459–494
43. Spence K, Venditti R, Rojas O, Habibi Y, Pawlak J (2010) Cellulose 17(4):835–848
44. Spinola SM, Cannon JG (1985) J Immunol Methods 81(1):161–165
45. Staros JV, Wright RW, Swingle DM (1986) Anal Biochem 156(1):220–222
46. Su TJ, Lu Thomas RK, Cui ZF, Penfold J (1998) J Phys Chem B 102(41):8100–8108
47. Syverud K, Stenius P (2009) Cellulose 16(1):75–85
48. Uschanov P, Johansson L, Maunu S, Laine J (2011) Cellulose 18(2):393–404
49. Wu P, Castner DG, Grainger DW (2008) J Biomater Sci Polym Ed 19(6):725–753
50. Yager P, Edwards T, Fu E, Helton K, Nelson K, Tam MR, Weigl BH (2006) Nature 442(7101):412–418
51. Yano H, Nakahara S (2004) J Mater Sci 39(5):1635–1638